AIAA JOURNAL
Vol. 42, No. 10, October 2004

Thermal/Mechanical Response of a Polymer Matrix Composite at Cryogenic Temperatures

Karen S. Whitley* and Thomas S. Gates†
NASA Langley Research Center, Hampton, Virginia 23681-0001

The mechanical behavior of a polymeric-matrix composite at cryogenic temperatures was investigated. Experimental data are presented on the residual mechanical properties of a carbon–fiber polymeric composite, IM7/PETI-5, both before and after aging. Both tension and compression modulus and strength were measured at room temperature, −196°C, and −269°C on five different laminate configurations consisting of $[0]_{12}$ and $[90]_{12}$ unidirectional laminates, $[\pm 25]_{3S}$ and $[\pm 45]_{3S}$ angle-ply laminates, and a 13-ply laminate [45/90/90/90/−45/0/0/0/−45/90/90/90/45]. One set of specimens was aged isothermally for 576 h at −184°C in an unconstrained state. Another set of corresponding specimens was aged under constant uniaxial strain for 576 hours at −184°C. Based on the experimental data presented, it is shown that trends in stiffness and strength that result from changes in temperature are not always smooth and consistent. Moreover, it is shown that loading mode and direction are significant for both stiffness and strength and that aging at cryogenic temperature while under load can alter the mechanical properties of pristine, unaged laminates made of IM7/PETI-5 material.

Introduction

NASA has recently initiated the Space Launch Initiative program that will, in part, advance some of the key technologies required for the next generation of launch vehicles. This next generation of space transportation systems may require both reusable launch vehicles (RLVs) and expendable launch vehicles (ELVs) to satisfy mission requirements. One of the key technologies identified for RLVs and ELVs has been the reduction in structural weight through the use of advanced materials and manufacturing methods. This reduction in structural weight must be tempered against the increased demands on performance, damage tolerance, and lifetime durability. One potential source for structural weight reduction is the replacement of traditional metallic cryogenic-fuel tanks with polymeric–matrix–composite (PMC) tanks.

The interest in design of polymeric-composite, cryogenic-fuel tanks for launch vehicles goes back several years and includes research associated with the National Aerospace Plane, single-stage-to-orbit vehicles[1,2] and other launch vehicle applications.[3] For internal and external tanks, design of the tank may take the form of externally stiffened shells of PMC material or thin-walled sandwich shells constructed with a lightweight core and PMC facesheets. Regardless of the design, the PMC-based tanks will be required to carry pressure and flight loads safely and to operate over temperatures that may range from −250 to +120°C. From a durability perspective, the primary performance criteria of the PMC material is to retain mechanical properties within allowable limits over the lifetime of the tank, while minimizing loss of cryogenic fuel due to permeation or leakage through the tank wall.

Aside from their use in space launch vehicles, there have been very few applications of PMCs as structural materials in cryogenic environments. Consequently, a review of the available literature provides a limited amount of experimental data on the mechanical properties of polymers or PMCs operating at cryogenic temperatures. For amorphous and crystalline polymeric materials, Perepechko[4] provides details on a number of nonmechanical properties that include thermal expansion and thermal conductivity, as well as viscoelastic or dynamic mechanical properties. From these studies, it is clear that many of the polymer properties are not linear with respect to temperature over a range from room temperature to approximately absolute zero. In the work by Pannkoke and Wagner,[5] fatigue tests were performed on unidirectional thermoplastic composites at −196°C. The fatigue strength at 10^6 cycles was found to be only 60% of the static strength. In this work, it was recognized that large thermal stresses degraded the fatigue performance. In a series of articles by Ahlborn,[6,7] static tests and thermally cycled and mechanically cycled tests were performed on unidirectional and cross-ply thermoplastic composites. Isothermal tests were performed at 23, −196, and −269°C, and cyclic thermal tests were performed between −196 and 23°C. Strength, damage, and fatigue life were measured for all test conditions. He found that the matrix-dominated properties, shear and transverse tension, were largely related to the effects of temperature on static strength. As the temperature decreased, increases in matrix-dominated strength could be offset by the development of thermal-stress-induced cracks. As in previous studies, the fatigue life was reduced as the test temperature was decreased.

More recently, a compilation of test data for several PMC material systems[8] indicated that tensile modulus, tensile strength, and compressive strength all generally increased as the test temperature was decreased from 23 to −269°C. Once again, it was found that thermal stresses had a large influence on behavior and that the sensitivity of matrix-dominated properties to temperature can be used to help explain the stress–strain response of laminated composites. Of these matrix-dominated properties, transverse-ply strength appears to play a critical role in the development and growth of residual stress-induced matrix cracks. Schoeppner et al.[9] recently investigated the range of thermomechanical loading over which steady-state matrix cracking is likely to occur. Shimoda[10] has performed additional studies related to matrix crack development in PMCs due to cryogenic-temperature exposure.

It is recognized that a broad spectrum of factors influence the mechanical properties of PMCs including material selection, composite fabrication and handling, aging or preconditioning, specimen preparation, laminate ply layup, test procedures, etc. The present study focuses on test temperature, preconditioning methods, and laminate configuration as the primary test variables. It is expected that by focusing on those three variables the results of this study will aid in the development of future material qualification methods and design verification testing. Toward that purpose, this paper provides experimental results and test methods developed from a series of

Presented as Paper 2002-1416 at the AIAA/ASME/ASCE/AHS/ASC 43rd Structures, Structural Dynamics, and Materials Conference, Denver, CO, 23 April 2002; received 7 March 2003; revision received 13 April 2004; accepted for publication 30 April 2004.

*Aerospace Engineer, Mechanics and Durability Branch.
†Senior Materials Research Engineer, Mechanics and Durability Branch. Associate Fellow AIAA.

thermal/mechanical tests. The selected test conditions represent a range of exposure times, loads, and temperatures similar to those experienced during the lifetime of a liquid-hydrogen fuel tank.

In particular, this paper first presents a description of the material system, IM7/PETI-5, and the material characterization test plan, including a description of the experimental methods that were used for tension and compression testing at room temperature and cryogenic temperatures. Also presented are the techniques used to precondition the IM7/PETI-5 material, followed by details on acquiring the residual property measurements. In addition, residual-stress analysis is used to evaluate thermal stresses as a function of ply layup, test temperature, and preconditioning. Results of the residual stiffness and strength are also evaluated as a function of ply layup, test temperature, and preconditioning. Finally, the fracture and edge surfaces are shown and discussed.

Material System

The IM7/PETI-5 material used in this study consisted of a continuous high-strength, intermediate-modulus, carbon fiber in a thermoplastic polyimide matrix. The IM7/PETI-5 material was considered as a suitable study material because it is high-temperature system that could lend itself to the design of a lightweight thermal protection system integrated to the composite tank and because its relatively high material toughness could potentially reduce the rate and density of laminate microcracking associated with tank permeability requirements. All test materials were laminated composites fabricated at the NASA Langley Research Center. These composite panels consisted of $[0]_{12}$ and $[90]_{12}$ unidirectional laminates, $[\pm 25]_{3S}$ and $[\pm 45]_{3S}$ angle-ply laminates, and a 13-ply laminate given by $[45/90_3/-45/\bar{0}_3]_S$. The bar notation over the 0 indicates that the 0_3 ply group spans the midplane of the laminate. Figure 1 provides a schematic illustrating the 0-deg ply and the 90-deg fiber directions relative to the specimen dimensions. These layups were chosen to provide basic lamina-level material constants and, for the case of the $[\pm 25]_{3S}$ and $[45/90_3/-45/\bar{0}_3]_S$ laminates, to be representative of a composite wall in a typical cryogenic-propellant tank. For a cryogenic tank, the orientation of 0 deg in the $[45/90_3/-45/\bar{0}_3]_S$ laminate would be along the longitudinal axis of the tank.

All composite panels were fabricated by hand layup. The bagging and cure processes employed are consistent with standard practices. Specifically, a full vacuum was applied to each bagged panel during the entire cure cycle. The cycle started with a ramp to 260°C, at 5°C/min. After a 1-h hold at 260°C, the autoclave was pressurized to 1480 kPa at 170 kPa/min while the temperature was increased to 370°C at 5°C/min. Then, the temperature was held at 370°C for 1 h, and the pressure was maintained until the temperature cooled to 38°C. After curing, through-transmission, ultrasonic inspection of the laminates indicated that there were no significant internal anomalies in any of the panels. The glass transition temperature T_g of the as-received composite material was 267°C, as measured by the peak in the tan δ curve of tests run in a dynamic mechanical analysis test.[11]

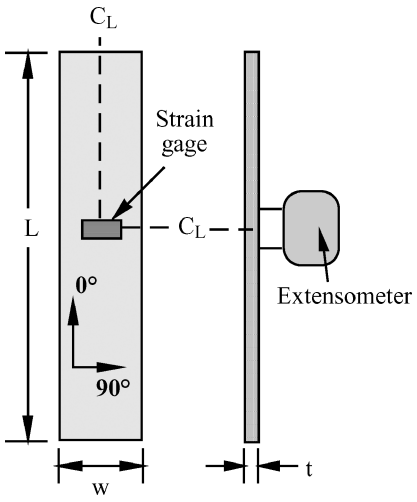

Fig. 1 Tensile specimen schematic; axial strain gauges mounted back-to-back on specimen, test temperatures 24, −196, and −269°C; $W = 25.4$, 19.0, and 19.0 mm; and $L = 152.4$, 254.0, and 254.0, respectively.

Material Characterization

The material characterization test plan consisted of two phases. The first phase addressed material aging where the material was subjected to long-term exposure at cryogenic temperature in either an unloaded (unconstrained) or statically loaded state. The second phase was residual property characterization of pristine and aged specimens at three temperatures (23, −196, and −269°C). This second phase provided fundamental material properties and an understanding of material behavior as a function of prior aging conditions and test temperatures. The complete test matrix, including the phase-1 aging conditions and the phase-2 residual property tests, are shown in Table 1.

All tests were conducted on coupon-type specimens that were cut from larger panels before aging. Three replicates of each condition were used to generate the test data. A schematic of the tension-test coupon is presented in Fig. 1. The 254-mm-long tension coupons were mounted in the test setup such that 63 mm of each end were gripped between two serrated faceplates, leaving a 128-mm test section. The faceplates were clamped together by using six hex-head bolts, which were torqued to 61 N · m with a hand-held torque wrench. The tensile coupons tested at room temperature were 152.4 mm long, and 38.1 mm of each end were mounted in hydraulic wedge grips, leaving a 76.2-mm test section.

The general set of guidelines used for the tension test included American Society for Testing and Materials (ASTM) D3039-76 and the Suppliers of Advanced Composite Materials (SACMA) SRM 4R-94 test method.[12] The tensile modulus was calculated by using ASTM D3039-76 and a linear regression least-squares curve fit of the stress–strain data in the linear region of the stress–strain curve. The linear region of the stress–strain curve was most commonly defined as being between $1000_{\mu\varepsilon}$ and $3000_{\mu\varepsilon}$ for all test conditions and specimen ply layups.

Because an existing end-loaded compression fixture, developed by Northrup Grumman, had been successfully used for previous compression testing of IM7/PETI-5 for the NASA High Speed Research Program,[13] it was selected as the fixture to be used for the compression testing in this study. A schematic of the compression coupon is presented in Fig. 2. The gauged coupon is placed in the center cutout section of the compression test fixture, as shown in Fig. 3a. A side view of the assembled fixture is shown in Fig. 3b. The compression tests were performed by using the SACMA recommended method, SRM 1R-94,[12] and the ASTM D695 references as guides. The compressive strength and modulus were calculated according to the method described in ASTM D695, by calculating the slope of the tangent to the initial linear portion of the stress–strain curve. In most cases, the linear region of the stress–strain curve from the compression test was defined as being between $1000_{\mu\varepsilon}$ and $2000_{\mu\varepsilon}$ for all test conditions and specimen ply layups.

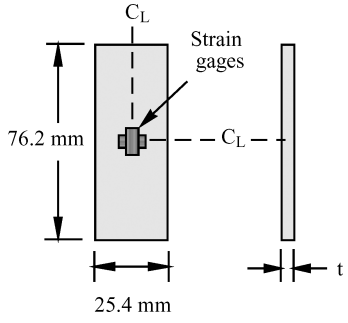

Fig. 2 Compression specimen schematic; stacked strain gauges mounted back-to-back on specimen.

Table 1 Test matrix illustrating the residual test temperature and aging condition for each type of laminate

	Aging condition (−184°C)		
Test temperature, °C	No load	Static load (3000 $\mu\varepsilon$)	Static load (4000 $\mu\varepsilon$)
24	$[0]_{12}$, $[90]_{12}$, $[\pm45]_{3S}$, $[\pm\underline{25}]_{3S}$, $[45/90_3/-45/\bar{0}_3]_S$	$[\pm45]_{12}$, $[0]_{12}$	$[\pm25]_{3S}$, $[45/90_3/-45/\bar{0}_3]_S$
−196	$[0]_{12}$, $[90]_{12}$, $[\pm45]_{3S}$, $[\pm\underline{25}]_{3S}$, $[45/90_3/-45/\bar{0}_3]_S$	$[\pm45]_{12}$, $[0]_{12}$	$[\pm25]_{3S}$, $[45/90_3/-45/\bar{0}_3]_S$
−269	$[0]_{12}$, $[90]_{12}$, $[\pm45]_{3S}$, $[\pm\underline{25}]_{3S}$, $[45/90_3/-45/\bar{0}_3]_S$	$[\pm45]_{12}$, $[0]_{12}$	$[\pm25]_{3S}$, $[45/90_3/-45/\bar{0}_3]_S$

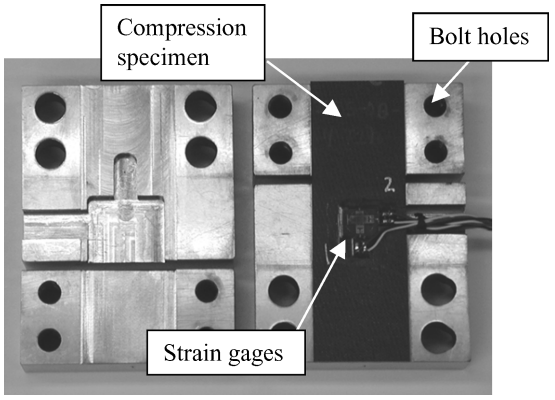

a) Open view

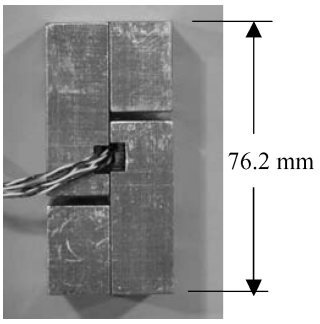

b) Side view

Fig. 3 Compression-test fixture.

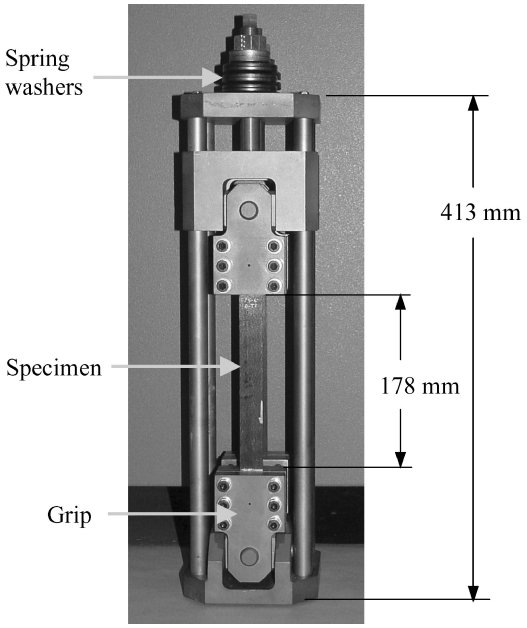

Fig. 4 Constant-strain fixture.

Test Phase 1: Material Aging

Another unique test fixture, also developed under the NASA High Speed Research Program, was used to produce a constant tensile-strain condition for half of the total number of specimens used during the aging phase. Several fixtures, like the one shown in Fig. 4, were constructed of Invar material [coefficient of thermal expansion (CTE) = 1.4×10^{-6}/°C] and could accommodate two rectangular specimens. The high stiffness of the fixture relative to the test specimen and the low CTE of the Invar material ensured a constant-strain condition during the entire aging period. The ability of the test fixture to maintain a constant strain within a specimen was verified by applying a preload to a gauged specimen mounted in the fixture and monitoring the strain while aging at −184°C. Each specimen was individually preloaded to the desired strain level by compressing a series of spring-type washers that react against the frame to put the specimen into tension. The washers were compressed by turning an adjacent nut with a hand held wrench, while the strain in the specimen was monitored with a longitudinal extensometer mounted on the specimen. The preload strain levels, given in Table 1, were selected to be approximately 50% of the not-aged room-temperature failure strain. A corresponding set of specimens was aged in an unconstrained condition. The constant-strain fixtures with specimens and the corresponding unconstrained specimens were placed into a large cryochamber that maintained a constant temperature of −184°C for an aging time of 576 h.

Test Phase 2: Residual Properties

In phase 2 of the test program, residual strength and stiffness of all three sets of specimens (pristine, aged without load, and aged with load) were measured at room temperature (24), −196 and −269°C. All residual-property tests were performed with a servohydraulic test machine, using a displacement rate of 1.27 mm/min. The isothermal cryogenic test conditions at −196 and −269°C were achieved by immersing the test specimen and load introduction apparatus into liquid nitrogen or liquid helium, respectively. To reach thermal equilibrium, the specimen stayed immersed in a constant level of the cryogen for at least 15 min before mechanical loading.

Stress in the test specimens was calculated by using load, as measured by the test-machine load cell, divided by the original cross section of the specimen. Strain in the tensile-test specimens was measured by using a combination of a cryogenic-rated axial extensometer (MTS Model 634.11F-21) and bonded electrical-resistance strain gauges (Measurements Group WK-00-250BG-350). Strain in the room-temperature compressive-test specimens was measured by using strain gauges, Measurements Group CEA-06-125WT-350, and the compression specimens was tested at cryogenic temperatures used Measurements Group WK-06-120WT-350 gauges. Strain gauge selection was based on considerations discussed in Ref. 14,

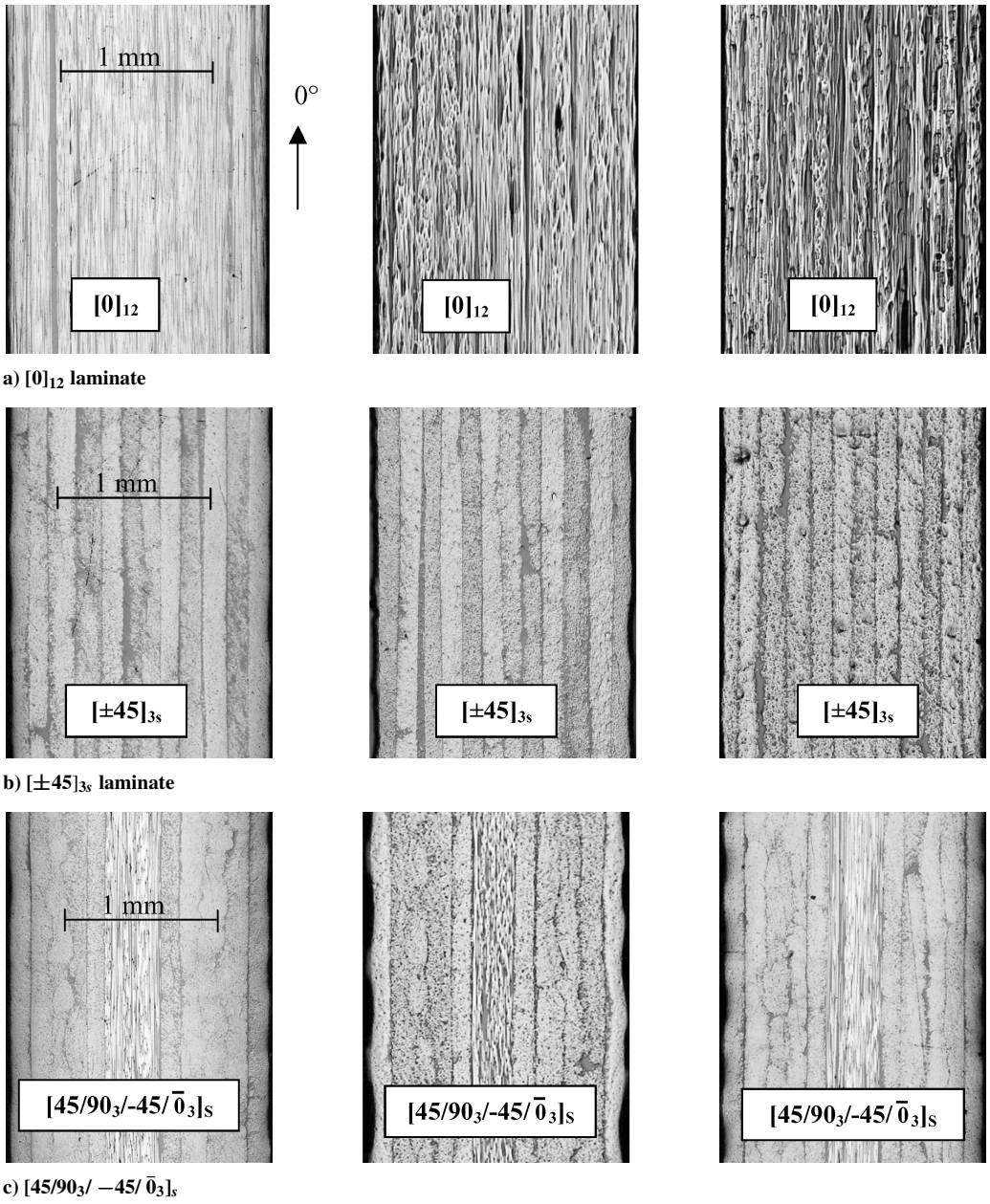

Fig. 5 Photomicrographs of specimen's edge before aging (left-hand side), after aging without load (center), and after aging with load (right-hand side).

such as material CTE, static-load test conditions, isothermal test temperatures, and gauge availability. The WK-series gauges are self-temperature-compensating to correct for thermal drift. Placement of these sensors on the tensile specimens is shown in Fig. 1, and placement on the compression specimen is shown in Fig. 2. All of the strain gauges were bonded in a back-to-back configuration.

Before aging, representative samples were polished along one edge. Sections (2.6 × 1.3 cm) were potted in a clear epoxy mold and were then circulated in an automated polishing wheel at 150 rpm with an applied weight of 2.27 kg per specimen. Consecutive grades of grit paper (600, 800, and 1200 grit) were used for the polishing. The specimens received a final polish with a solution of silica alumina suspension fluid. The polished specimen edges were examined for damage (microcracks and delaminations) using optical microscopy, and photomicrographs were taken to establish the baseline condition. After aging, but before the destructive residual tests, visual examination of all layups was again performed to determine if the exposure conditions generated any microcracks, damage, or change in surface morphology. Photomicrographs representative of the specimen's edge before and after aging are shown in Fig. 5.

Residual-Stress Analysis

The previous studies cited herein indicate that thermal stresses alone may degrade laminate performance. For thermal loading, stresses are induced at the ply level by mismatches in expansion or contraction of ply constituents and by constraining effects caused by adjacent plies that prevent a free relative expansion or contraction. The residual stresses in any ply can be calculated by using classical laminated plate theory.[15] In general, for a unidirectional laminate under plane stress, the constitutive relationship is given by

$$\begin{Bmatrix}\sigma_{11}\\ \sigma_{22}\\ \sigma_{12}\end{Bmatrix} = \begin{bmatrix}Q_{11} & Q_{12} & 0\\ Q_{12} & Q_{22} & 0\\ 0 & 0 & Q_{66}\end{bmatrix}\left(\begin{Bmatrix}\varepsilon_{11}\\ \varepsilon_{22}\\ \gamma_{12}\end{Bmatrix} - \begin{Bmatrix}\varepsilon_{11}^{T}\\ \varepsilon_{22}^{T}\\ \gamma_{12}^{T}\end{Bmatrix}\right) \quad (1)$$

where σ_{ij} are the normal stress components in the principal material directions, ε_{ij} are the normal strains in the principal material directions, and Q_{ij} are the reduced stiffness coefficients. In this equation, the subscripts 1 and 2 denote the fiber direction and in-plane direction perpendicular to the fiber, respectively. The thermal strains, in

the principal material directions, ε_{ij}^T, are calculated using

$$\begin{Bmatrix} \varepsilon_{11}^T \\ \varepsilon_{22}^T \\ \gamma_{12}^T \end{Bmatrix} = \begin{Bmatrix} \alpha_1 \\ \alpha_2 \\ 0 \end{Bmatrix} \Delta T \tag{2}$$

The thermal strains are proportional to the temperature change ΔT, which is the temperature difference between the test condition and the stress-free condition at cure. In Eq. (2), CTE, α_1 and α_2, are assumed to be constant over the range of temperature. The thermal shear strain γ_{12}^T is zero because an orthotropic material only exhibits dilation along its principal material coordinate directions, with a change in temperature. Clearly, from Eq. (2), it is apparent that for large values of ΔT, which occur at cryogenic temperatures, the magnitude of the thermally induced strains is highly dependent on the material CTE values. In particular, nonlinear behavior of the CTE with respect to temperature, as shown in Table 2 from Ref. 16, may result in residual thermal stresses that also vary in a nonlinear manner with respect to temperature. To illustrate this effect, CTE values and material properties given in Table 3 were used with classical laminated plate theory to predict the maximum transverse ply stress σ_{22} as a function of laminate stacking sequence, test temperature, and laminate preconditioning. The results of these calculations are given in Table 4. In effect, this was a piecewise calculation based on a known value of CTE at a given temperature. If the CTE values as a function of temperature were represented as a continuous function, then Eq. (2) could be modified within the context of lamination theory to account for residual stresses at temperatures between the measurement points. Note that CTE values of pristine material were used for all conditions and the stress-free temperature was assumed to be the glass transition temperature of IM7/PETI-5. With respect to temperature, Table 4 indicates that the trend for the not-aged condition is for the transverse stress to increase with a decrease in temperature. However, both of the isothermal-aged conditions predict the largest stress (σ_{22}) to occur at the intermediate temperature, −196°C. With respect to ply layup, the highly constrained $[45/90_3/-45/\bar{0}_3]_S$ laminate is predicted to have the highest stress at any given temperature. However, the $[\pm 45]_{3S}$ angle-ply laminate is predicted to have stress magnitudes close to those predicted for the $[45/90_3/-45/\bar{0}_3]_S$ laminate. With respect to preconditioning, no clear trends are evident from a residual-stress analysis.

Table 2 CTE for not-aged IM7/PETI-5 material system

	× 10^{-6}/°C	
Temperature, °C	α_1	α_2
24	−1.30	19.45
−196	−1.49	20.05
−273	−2.77	18.46

Results and Discussion

In this section, elastic modulus and residual strength results are presented for laminates with $[0]_{12}$, $[\pm 25]_{3S}$, $[45/90_3/-45/\bar{0}_3]_S$, [90]12, and $[\pm 45]_{3S}$ ply stacking sequences. Tables 3 and 5 contain the tensile and compressive elastic modulus, respectively, at the three different test temperatures, for each layup and for each aging condition. Each value in Tables 3 and 5 represents the average of three replicates, along with the standard deviation. The lamina in-plane moduli values, E_1 and E_2, were calculated directly from stress–strain behavior of the $[0]_{12}$ and $[90]_{12}$ unidirectional laminates, respectively. The laminate effective modulus value E_x of the $[\pm 25]_{3S}$ and $[45/90_3/-45/\bar{0}_3]_S$ laminates was calculated from the laminate stress–strain behavior. The lamina in-plane shear modulus G_{12} was calculated indirectly from the stress–strain behavior of the $[\pm 45]_{3S}$ laminates by using the equation

$$G_{12} = E_x/2(1 + \nu_{xy}) \tag{3}$$

where ν_{xy} is the laminate Poisson's ratio and E_x is the laminate longitudinal modulus. The form of Eq. (3) is customarily associated with isotropic materials; however, for the special case of a $[\pm 45]_S$ laminate subjected to axial loading, the shear modulus can be calculated by using this equation.[17]

Measured laminate tensile and compressive strength values are listed in Tables 6 and 7, respectively, along with the associated standard deviation. Failure was defined as the point of complete loss of load-carrying capability during the test. Because of the nonlinear nature of the stress–strain behavior in the $[\pm 45]_{3S}$ laminates,

Table 4 Calculated maximum transverse ply stress σ_{22} for thermal loading only

	Maximum transverse ply stress, MPa			
Temperature, °C	$[0]_{12}$	$[\pm 25]_{3S}$	$[45/90_3/-45/\bar{0}_3]_S$	$[\pm 45]_{3S}$
	Not aged			
24	0.0	18.2	41.3	40.6
−196	0.0	37.7	70.9	69.7
−269	0.0	45.7	83.7	82.3
	Isoaged without load			
24	0.0	18.9	40.8	40.1
−196	0.0	43.6	88.3	86.5
−269	0.0	40.8	76.5	75.3
	Isoaged with load			
24	0.0	20.4	40.7	39.9
−196	0.0	43.1	89.3	87.5
−269	0.0	42.9	76.9	75.8

Table 3 Measured tensile elastic modulus values

Specimen ply layup	Temperature, °C	Material property	Not aged modulus ± standard deviation, GPa	Aged without load modulus ± standard deviation, GPa	Aged with load modulus ± standard deviation, GPa
$[0]_{12}$	24	E_1	157.6 ± 9.3	153.6 ± 5.9	147.2 ± 2.6
$[0]_{12}$	−196	E_1	151.6 ± 2.2	146.3 ± 11.5	149.2 ± 1.9
$[0]_{12}$	−269	E_1	145.1 ± 7.4	143.0 ± 8.8	158.6 ± 20.8
$[\pm 25]_{3S}$	24	E_x	71.9 ± 1.0	70.3 ± 1.6	59.8 ± 2.6
$[\pm 25]_{3S}$	−196	E_x	75.7 ± 0.8	63.8 ± 8.5	71.5 ± 3.0
$[\pm 25]_{3S}$	−269	E_x	73.1 ± 3.7	69.4[a]	65.6 ± 12.2
$[45/90_3/-45/\bar{0}_3]_S$	24	E_x	50.7 ± 1.0	46.7 ± 4.3	51.0 ± 1.1
$[45/90_3/-45/\bar{0}_3]_S$	−196	E_x	40.6 ± 5.9	48.0 ± 1.8	48.6 ± 3.0
$[45/90_3/-45/\bar{0}_3]_S$	−269	E_x	43.8 ± 1.9	44.3 ± 3.9	52.1 ± 1.3
$[90]_{12}$	24	E_2	8.7 ± 0.1	8.6 ± 0.1	NA
$[90]_{12}$	−196	E_2	7.5 ± 0.1	9.5 ± 2.0	9.6 ± 0.1
$[90]_{12}$	−269	E_2	7.8 ± 1.2	7.1 ± 0.8	NA
$[\pm 45]_{3S}$	24	G_{12}	4.6 ± 0.4	5.0 ± 0.1	5.8 ± 0.2
$[\pm 45]_{3S}$	−196	G_{12}	5.8 ± 0.1	6.2 ± 0.1	6.0 ± 0.2
$[\pm 45]_{3S}$	−269	G_{12}	6.2 ± 0.2	5.5 ± 0.9	6.1 ± 0.3

[a]Only one specimen tested.

Table 5 Measured compressive elastic modulus values

Specimen ply layup	Temperature, °C	Material property	Not aged modulus ± standard deviation, GPa	Aged without load modulus ± standard deviation, GPa	Aged with load modulus ± standard deviation, GPa
$[0]_{12}$	24	E_1	135.2 ± 1.1	139.0 ± 3	129.9 ± 4.8
$[0]_{12}$	−196	E_1	142.0 ± 15.0	154.0 ± 5.9	147.9 ± 5.5
$[0]_{12}$	−269	E_1	146.9 ± 11.1	143.1 ± 6.0	139.9 ± 11.4
$[\pm 25]_{3S}$	24	E_x	63.2 ± 5.7	60.0 ± 4.1	62.8 ± 3.1
$[\pm 25]_{3S}$	−196	E_x	64.1 ± 7.5	72.1 ± 8.0	72.6 ± 2.5
$[\pm 25]_{3S}$	−269	E_x	77.5 ± 17.5	77.3 ± 9.4	69.5 ± 1.7
$[45/90_3/-45/\bar{0}_3]_S$	24	E_x	44.3 ± 5.1	46.3 ± 0.9	40.7 ± 7.6
$[45/90_3/-45/\bar{0}_3]_S$	−196	E_x	60.6 ± 7.3	50.8 ± 4.8	52.2 ± 7.0
$[45/90_3/-45/\bar{0}_3]_S$	−269	E_x	51.2 ± 4.2	47.6 ± 1.1	53.7 ± 5.0
$[90]_{12}$	24	E_2	11.6 ± 1.7	12.1 ± 0.5	NA
$[90]_{12}$	−196	E_2	11.9 ± 1.1	11.1 ± 0.5	NA
$[90]_{12}$	−269	E_2	12.8 ± 1.1	12.2 ± 01.6	NA
$[\pm 45]_{3S}$	24	G_{12}	4.8 ± 2.5	5.3 ± 0.5	4.3 ± 0.1
$[\pm 45]_{3S}$	−196	G_{12}	6.7 ± 0.8	5.4 ± 0.5	6.0 ± 1.2
$[\pm 45]_{3S}$	−269	G_{12}	7.6 ± 3.0	5.8 ± 0.3	7.0 ± 2.0

Table 6 Measured tensile strength values

Specimen ply layup	Temperature, °C	Not aged strength ± standard deviation, MPa	Aged without load strength ± standard deviation, MPa	Aged with load strength ± standard deviation, MPa
$[0]_{12}$	24	1939.8 ± 276.3	1864.8 ± 42.42	1847.8 ± 49.4
$[0]_{12}$	−196	1277.9 ± 207.5	1567.7 ± 39.0	1536.1 ± 125.8
$[0]_{12}$	−269	1495.2 ± 326.2	1451.0 ± 275.1	1771.4 ± 186.3
$[\pm 25]_{3S}$	24	1132.2 ± 76.8	1265.9 ± 57.8	954.9 ± 83.8
$[\pm 25]_{3S}$	−196	911.6 ± 49.5	902.4 ± 208.1	1119.5 ± 51.4
$[\pm 25]_{3S}$	−269	1130.7 ± 15.0	1113.6[a]	1024.4 ± 209.2
$[45/90_3/-45/\bar{0}_3]_S$	24	711.0 ± 14.0	699.9 ± 67.0	842.6 ± 37.9
$[45/90_3/-45/\bar{0}_3]_S$	−196	585.4 ± 118.7	747.9 ± 57.1	872.4 ± 39.7
$[45/90_3/-45/\bar{0}_3]_S$	−269	656.5 ± 47.6	731.8 ± 64.4	806.1 ± 2.1
$[90]_{12}$	24	46.7 ± 1.9	46.6 ± 3.0	NA
$[90]_{12}$	−196	21.0 ± 3.5	23.5 ± 30.1	63.1 ± 4.9
$[90]_{12}$	−269	17.5 ± 3.9	11.3 ± 4.7	NA
$[\pm 45]_{3S}$[b]	24	162.7 ± 2.3	165.0 ± 0.5	182.0 ± 4.3
$[\pm 45]_{3S}$	−196	241.6 ± 3.7	249.0 ± 3.0	245.4 ± 7.7
$[\pm 45]_{3S}$	−269	255.9 ± 8.2	257.0 ± 11.9	257.0 ± 4.7

[a]Only one specimen tested. [b]Tensile strength defined as the initial point of deviation from the tangent of the nearly horizontal slope of the stress strain curve.

Table 7 Measured compressive strength values

Specimen ply layup	Temperature, °C	Not aged strength ± standard deviation, MPa	Aged without load strength ± standard deviation, MPa	Aged with load strength ± standard deviation, MPa
$[0]_{12}$	24	857.5 ± 52.5	856.2 ± 102.4	817.4 ± 74.2
$[0]_{12}$	−196	1124.8 ± 127.6	1167.2 ± 60.9	1115.2 ± 66.2
$[0]_{12}$	−269	1193.5 ± 100.8	1234.7 ± 44.6	1156.1 ± 61.0
$[\pm 25]_{3S}$	24	502.9 ± 65.7	467.7 ± 37.2	524.8 ± 43.4
$[\pm 25]_{3S}$	−196	604.2 ± 9.6	709.5 ± 0.3	685.6 ± 87.2
$[\pm 25]_{3S}$	−269	714.8 ± 132.7	749.4 ± 27.2	571.2 ± 61.5
$[45/90_3/-45/\bar{0}_3]_S$	24	473.3 ± 121.8	432.6 ± 10.2	530.6 ± 107.5
$[45/90_3/-45/\bar{0}_3]_S$	−196	375.7 ± 130.1	554.3 ± 29.8	709.5 ± 89.2
$[45/90_3/-45/\bar{0}_3]_S$	−269	572.2 ± 28.6	619.1 ± 11.9	723.0 ± 113.4
$[90]_{12}$	24	220.0 ± 10.0	280.0 ± 11.5	NA
$[90]_{12}$	−196	293.7 ± 16.1	273.7 ± 52.7	NA
$[90]_{12}$	−269	367.6 ± 35.1	301.9 ± 21.8	NA
$[\pm 45]_{3S}$	24	426.7 ± 27.7	398.3 ± 26.4	364.8 ± 12.2
$[\pm 45]_{3S}$	−196	536.8 ± 73.3	511.0 ± 57.1	530.5 ± 21.4
$[\pm 45]_{3S}$	−269	578.1 ± 13.8	569.5 ± 10.38	454.6 ± 98.0

their tensile strength was defined as the initial point of deviation from the nearly horizontal portion of the stress–strain curve. Normalized tensile modulus and strength of the $[0]_{12}$, $[\pm 45]_{3S}$, and $[45/90_3/-45/\bar{0}_3]_S$ laminates are presented in Figs. 6–11 and normalized compressive modulus and strength are presented in Figs. 12–17. Both modulus and strength values have been normalized against the corresponding results for the not-aged condition tested at room temperature for each laminate.

Effect of Temperature on Modulus and Strength

When the results from specimens subjected to the not-aged test condition were examined, the effects of temperature on tensile modulus and strength were found. The fiber-dominated $[0]_{12}$ laminate experienced a decrease in both the modulus and strength due to testing at cryogenic temperatures, with up to a 35% decrease in strength for the −196°C case. Conversely, the shear modulus and longitudinal strength of the matrix-dominated $[\pm 45]_{3S}$ laminate increased

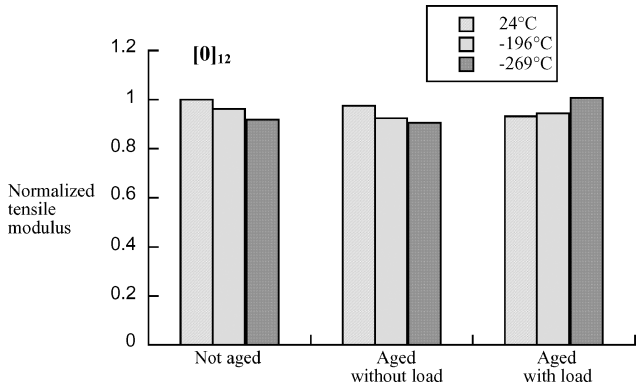

Fig. 6 Tensile modulus of $[0]_{12}$ specimens normalized against not-aged condition tested at room temperature.

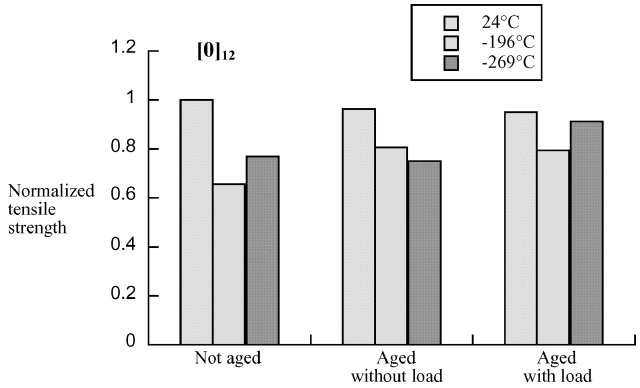

Fig. 7 Tensile strength of $[0]_{12}$ specimens normalized against not-aged condition tested at room temperature.

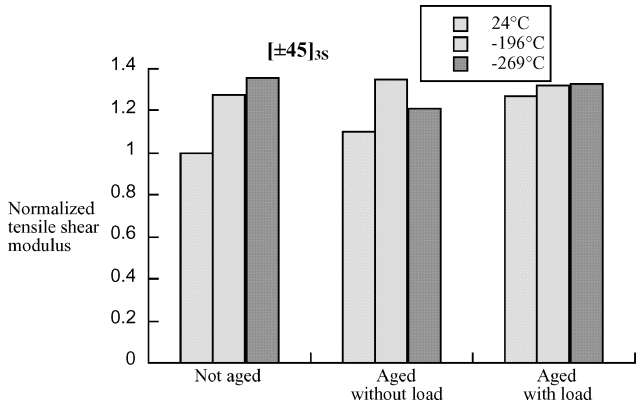

Fig. 8 Shear tensile modulus of $[\pm 45]_{3S}$ specimens normalized against not-aged condition tested at room temperature.

as the temperature decreased. The shear modulus increased by as much as 35% and the strength by as much as 50% when tested at −269°C. The transverse modulus E_2 showed a slight decline at cryogenic temperatures, whereas the transverse strength dropped by approximately 70% when the temperature was reduced to −269°C. The tensile modulus and strength of the not-aged $[45/90_3/-45/\bar{0}_3]_S$ laminates decreased by nearly 20% at −196°C, with some reverse in this decline as the temperature was lowered to −269°C. The $[\pm 25]_{3S}$ laminates showed little sensitivity in modulus or strength to cryogenic temperature.

The compressive modulus and strength increased for all of the laminates that were tested at cryogenic temperatures. In most cases, the highest modulus and strength occurred at the lowest test temperature (−269°C). Of all of the laminates tested, the $[90]_{12}$ laminates experienced the greatest increase (67%) in strength, whereas the $[\pm 45]_{3S}$ laminates experienced the greatest increase (57%) in modulus at cryogenic temperatures.

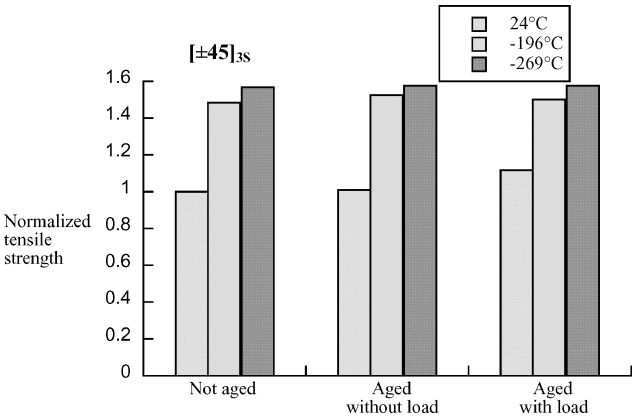

Fig. 9 Tensile strength of $[\pm 45]_{3S}$ specimens normalized against not-aged condition tested at room temperature.

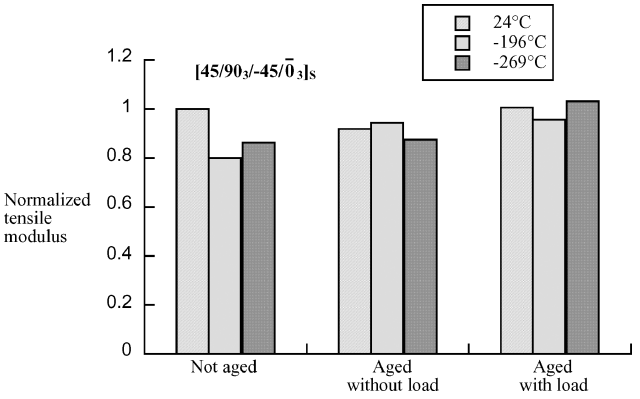

Fig. 10 Tensile modulus of $[45/90_3/-45/\bar{0}_3]_S$ specimens normalized against not-aged condition tested at room temperature.

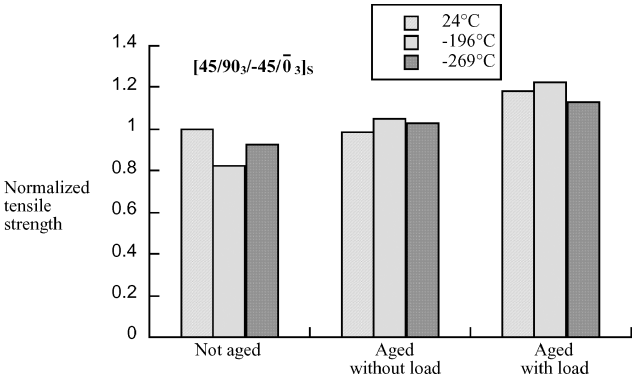

Fig. 11 Tensile strength of $[45/90_3/-45/\bar{0}_3]_S$ specimens normalized against not-aged condition tested at room temperature.

Effect of Aging on Modulus and Strength

To determine the effects of aging, the panels subjected to the not-aged condition were compared to the corresponding panels subjected to the aged-without-load and the aged-with-load conditions. The results show that, in general, aging had very little effect on the tensile modulus of the fiber-dominated $[0]_{12}$ laminate. Aging did cause a slight increase in tensile strength for the $[0]_{12}$ laminate, with the most significant change occurring when tested at −269°C after aging with load. In contrast, aging did not significantly affect the shear modulus or the longitudinal strength of the matrix-dominated $[\pm 45]_{3S}$ laminate.

For the $[45/90_3/-45/\bar{0}_3]_S$ laminate, aging increased the modulus. The $[45/90_3/-45/\bar{0}_3]_S$ laminate that was aged with load experienced the largest increase (18%) in modulus, which occurred at −269°C. Aging also increased the strength of the

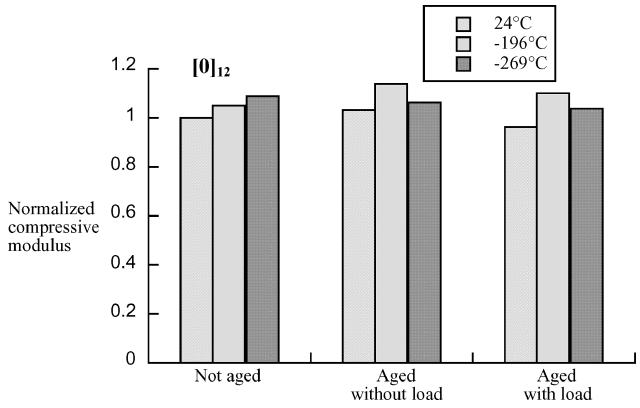

Fig. 12 Compressive modulus of $[0]_{12}$ specimens normalized against not-aged condition tested at room temperature.

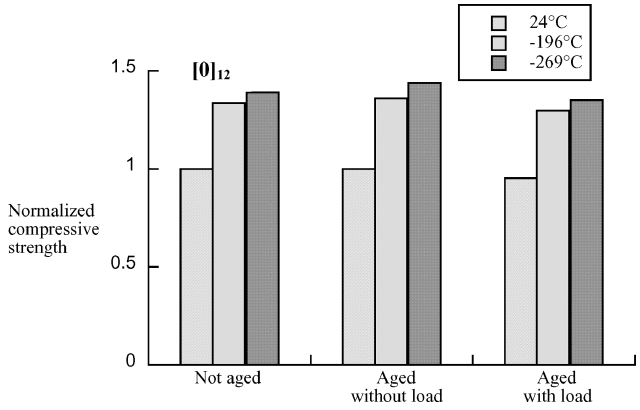

Fig. 13 Compressive strength of $[0]_{12}$ specimens normalized against not-aged condition tested at room temperature.

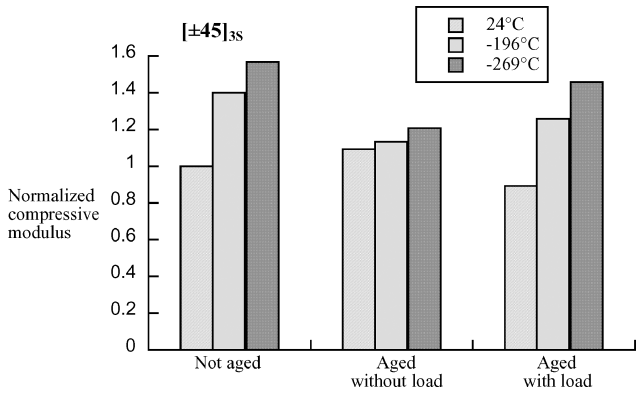

Fig. 14 Compressive modulus of $[\pm 45]_{3S}$ specimens normalized against not-aged condition tested at room temperature.

$[45/90_3/-45/\bar{0}_3]_S$ laminate, with the most significant increase occurring for the aged-with-load condition, where the strength increased relative to the baseline strength by 21% at -196°C and 11% at -269°C. In general, aging decreased the modulus of the $[\pm 25]_{3S}$ laminate and had little effect on the laminate strength. From the limited data for the $[90]_{12}$ laminate, it appears that aging had little effect on the transverse modulus and the strength.

As expected, the standard deviation in strength measurements was more significant than the standard deviation associated with modulus measurements. In part, large standard deviations in the strength values can be attributed the fact that strength is defined by a single value, whereas modulus is an averaged value, given by the slope of the stress–strain curve. Strength in laminated composites is also more sensitive to processing, handling, and test-parameter variability.

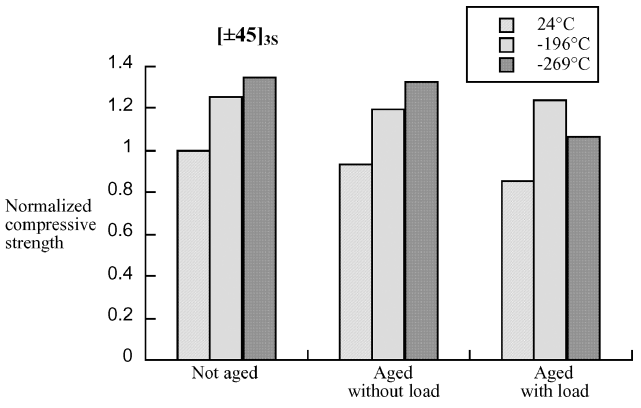

Fig. 15 Compressive strength of $[\pm 45]_{3S}$ specimens normalized against not-aged condition tested at room temperature.

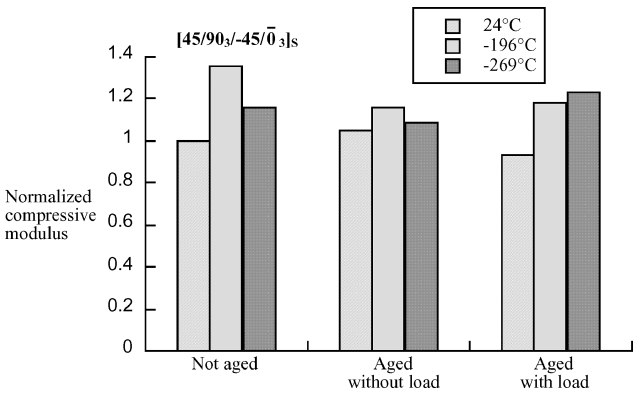

Fig. 16 Compressive modulus of $[45/90_3/-45/\bar{0}_3]_S$ specimens normalized against not-aged condition tested at room temperature.

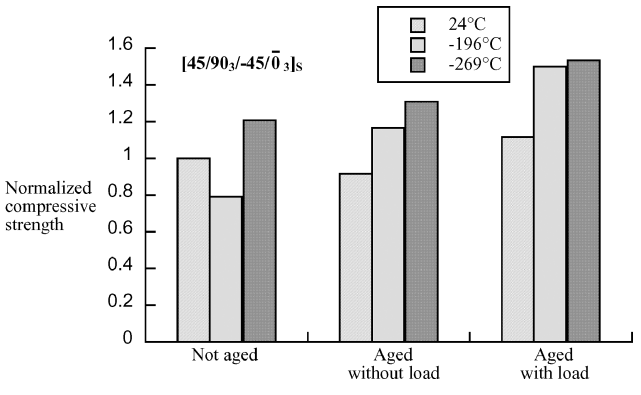

Fig. 17 Compressive strength of $[45/90_3/-45/\bar{0}_3]_S$ specimens normalized against not-aged condition tested at room temperature.

The compressive modulus and strength of the $[0]_{12}$ laminate were not greatly influenced by aging. The matrix-dominated $[\pm 45]_{3S}$ laminate showed a decrease in modulus and strength due to aging in most cases, and in general, the modulus decreased more than the strength. The compressive modulus of the $[45/90_3/-45/\bar{0}_3]_S$ laminate tended to decrease after aging. However, the compressive strength of the $[45/90_3/-45/\bar{0}_3]_S$ laminate increased due to aging. The greatest increase, 88%, occurred at -269°C after aging with load; however, the standard deviation associated with those strength values was quite high. The room-temperature modulus and strength of the $[\pm 25]_{3S}$ laminate were unaffected by aging. However, at -196°C, both the modulus and the strength increased due to aging. The $[90]_{12}$ laminate was not significantly affected by aging.

Fracture Surfaces

The fracture surfaces of each failed specimen were examined for any distinguishing features that could be attributed to test temperature or aging conditions. It was observed that aging did not produce any distinguishing characteristics in the fracture surfaces of the tensile specimens. The greatest distinction in the appearance was observed when comparing the fracture surfaces of the room-temperature test specimens with those of the cryogenic-temperature test specimens. However, there were no discernible differences between the specimens tested at −196°C and the specimens tested at −269°C.

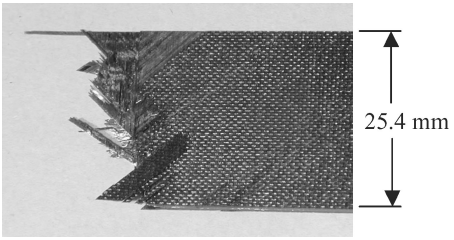

Fig. 18 Fracture surface of $[45/90_3/-45/\bar{0}_3]_S$ laminate after tensile test at room temperature.

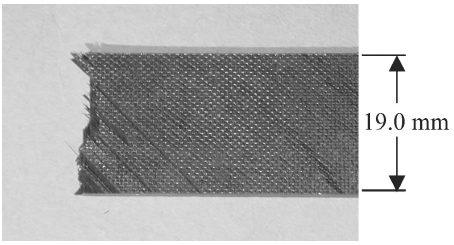

Fig. 19 Fracture surface of $[45/90_3/-45/\bar{0}_3]_S$ laminate after tensile test at −196°C.

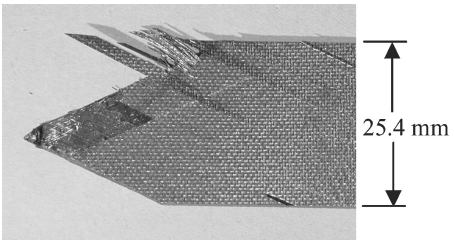

Fig. 20 Fracture surface of $[\pm 25]_{3S}$ laminate after tensile test at room temperature.

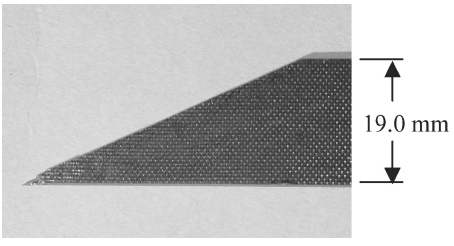

Fig. 21 Fracture surface of $[\pm 25]_{3S}$ laminate after tensile test at −196°C.

The fracture surface of the $[45/90_3/-45/\bar{0}_3]_S$ laminates tested at room temperature and −196°C are shown in Figs. 18 and 19, respectively. The fractured edge of the $[45/90_3/-45/\bar{0}_3]_S$ laminates tested at room temperature appeared more jagged, such that the ±45-deg laminas were more apparent. The $[45/90_3/-45/\bar{0}_3]_S$ laminates tested at −196°C failed such that the fracture surface was nearly perpendicular to the direction of the applied load. The $[\pm 25]_{3S}$ laminates tested at room temperature (Fig. 20) displayed irregular fracture surfaces, whereas the $[\pm 25]_{3S}$ laminates tested at −196°C displayed a very clean-cut failure at a 25-deg angle that is shown in Fig. 21. All of the $[0]_{12}$ laminates failed by splitting along the 0-deg direction. The $[0]_{12}$ laminates tested at room temperature displayed a catastrophic splintering as shown in Fig. 22, whereas the $[0]_{12}$ laminates (Fig. 23) tested at −196°C were characterized by only a few splits through the thickness. In general, the failure of the $[45/90_3/-45/\bar{0}_3]_S$, $[\pm 25]_{3S}$, and the $[0]_{12}$ laminates at cryogenic temperatures could be described as clean breaks, as opposed to the irregular fragmented breaks that occurred at room temperature. The clean breaks indicate that a more brittle fracture occurred at cryogenic temperatures, and the irregular breaks indicate that a more ductile fracture occurred at room temperature. There was no difference in the fracture surface of the $[90]_{12}$ laminates, which all failed straight across the width of the specimen in the 90-deg direction, regardless of the test temperature. Because of the nonlinear stress–strain behavior of the $[\pm 45]_{3S}$ laminate, loading to the point of fracture did not always occur.

The fracture surfaces of the specimens tested in compression did not show any differences due to test temperature or aging conditions, possibly because the test fixture enclosed most of the compression coupon. However, each set of laminate configurations displayed unique failure characteristics, as expected. In all cases, failure occurred contiguously above or below the strain-gauge section. The $[0]_{12}$-laminate compression failures did not split along the length, as in the tension tests. Instead, the fracture surface could be described as having a short broomlike appearance along the failed edge (Fig. 24). The $[90]_{12}$ laminates failed with a clean-cut, beveled edge across the width (Fig. 25). The $[\pm 25]_{3S}$ laminates failed sharply along a ±25 deg angle ply, and failure may have propagated from any one of the four corners of the specimen (Fig. 26). The $[45/90_3/-45/\bar{0}_3]_S$ laminate failed straight across the width of the specimen, with the fracture surface having a crushed appearance (Fig. 27).

Edge Surface Morphology

Optical examination of surface morphology was intended to provide data on the initiation and growth of any damage that occurred during specimen aging. Photomicrographs of the specimen's polished edges taken during this study are shown in Fig. 5. The photographs, in the first column are for the not-aged material, the second column are specimens that have been aged without load, and the third column are specimens that have been aged with load. Very few microcracks or similar damage were observed before or after aging in any of the layups. However, the surface morphology shows some definite degradation along the exposed edges after aging without

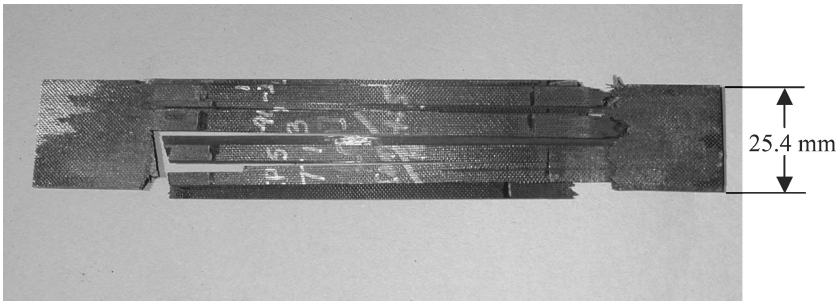

Fig. 22 Fracture surface of $[0]_{12}$ laminate after tensile test at room temperature.

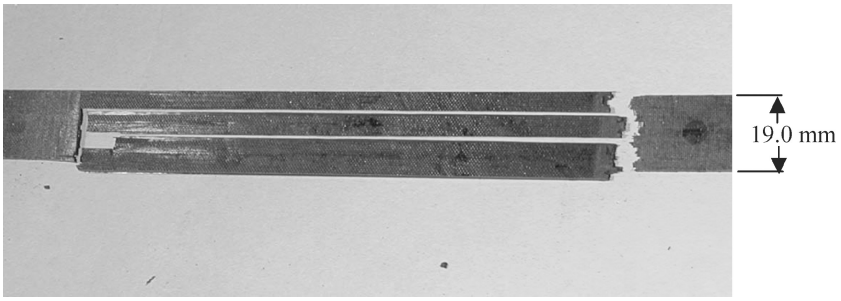

Fig. 23 Fracture surface of $[0]_{12}$ laminate after tensile test at −196°C.

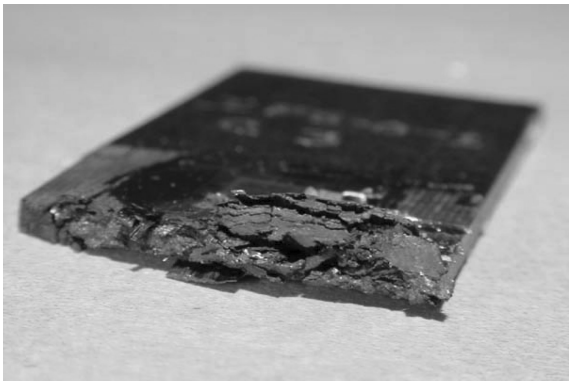

Fig. 24 Fracture surface of $[0]_{12}$ laminate after compression test at room temperature.

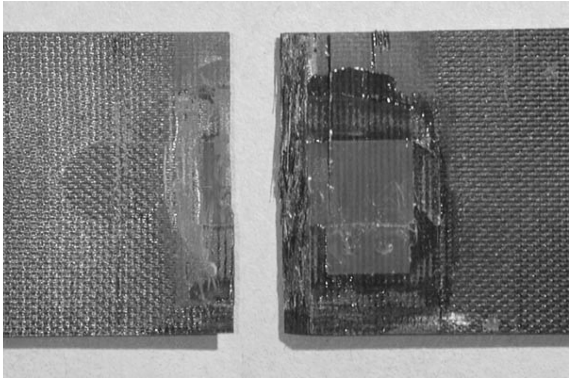

Fig. 25 Fracture surface of $[90]_{12}$ laminate after compression test at room temperature.

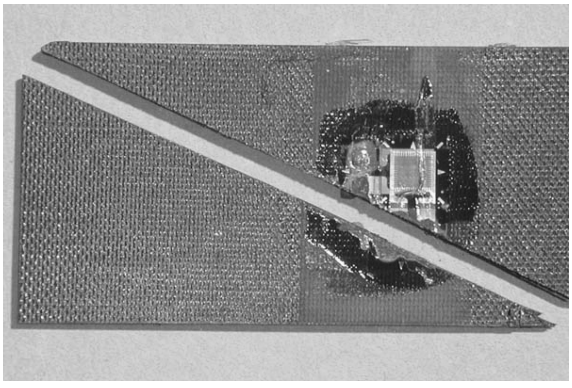

Fig. 26 Fracture surface of $[\pm 25]_{3S}$ laminate after compression test at room temperature.

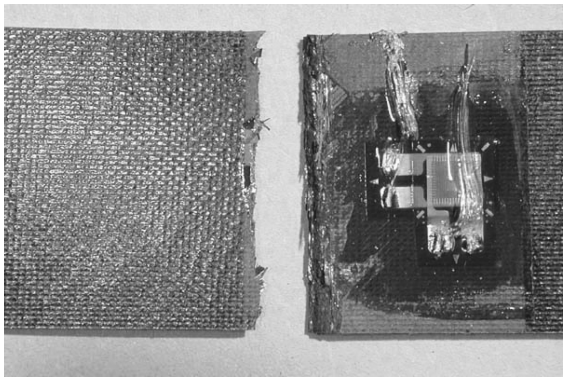

Fig. 27 Fracture surface of $[45/90_3/-45/\bar{0}_3]_S$ laminate after compression test at room temperature.

load, and it appears that further surface degradation occurred after aging with load. This degradation occurred in all layups and can be described as pitting in the matrix regions.

Conclusions

Five different laminates made of IM7/PETI-5 were evaluated for tensile and compressive strength and stiffness at room temperature and at two cryogenic temperatures. The effects of laminate configuration, test temperature, and preconditioning or aging were investigated. Examination of the basic laminate properties indicates that cryogenic temperatures can have an appreciable influence on behavior, as expected, but unexpected trends can occur, indicating that tests should be run at several temperature levels. For example, the tension-test data show that the longitudinal and transverse stiffness and strength decreased as the test temperature decreased. Conversely, the tensile shear modulus and strength increased as the temperature decreased. For compression loads, exposure to cryogenic temperatures produced an increase in both the modulus and strength of all of the laminates.

Aging the material at a constant cryogenic temperature caused changes in the strength and stiffness, compared to the corresponding values for the not-aged or as-received condition. In general, it appears that this type of aging will increase both the tensile strength and stiffness, particularly in the $[\pm 45]_{3S}$, $[90]_{12}$, and $[45/90_3/-45/\bar{0}_3]_S$ laminates. The aging tends to decrease the compressive strength and stiffness in the $[\pm 45]_{3S}$, $[90]_{12}$, and the $[0]_{12}$ laminates. Likewise, aging or long-term exposure at a cryogenic temperature while under load can alter mechanical properties of the as-received laminate, implying that design values should take into account thermomechanical exposure over the lifetime of the structure.

Based on lamination theory, residual-stress calculations indicate that the transverse tensile ply stresses, associated with matrix cracking, can be quite high at cryogenic test temperatures, which is important because these transverse residual stresses may reduce the strength and stiffness of the laminates by accelerating the initiation, growth, and accumulation of transverse microcracks.

Acknowledgments

The authors express their thanks to Lisa Hawks, Everitt Brown, and Charles Townsley of NASA Langley Research Center for their technical support.

References

[1]Morino, Y., Ishikawa, T., Aoki, T., Kumaza, H., and Hayashi, Y., "Feasibility Study of CFRP Material Application to the Cryogenic Propellant Tank of Reusable Launch Vehicles," *Proceedings of the 6th Japan International SAMPE Symposium*, Society for the Advancement of Material and Process Engineering, Tokyo, 1999, pp. 1127–1130.

[2]Robinson, M. J., "Composite Structures on the DC-XA Reusable Launch Vehicle," *Proceedings of the 28th International SAMPE Technical Conference*, Society for the Advancement of Material and Process Engineering, Seattle, WA, 1996.

[3]Callaghan, M. T., "Use of Resin Composites for Cryogenic Tankage," *Cryogenics*, Vol. 31, No. 4, 1991, pp. 282–287.

[4]Perepechko, I., *Low-Temperature Properties of Polymers*, Mir, Moscow, 1997, Chap. 3.

[5]Pannkoke, K., and Wagner, H. J., "Fatigue Properties of Unidirectional Carbon Fiber Composites at Cryogenic Temperatures," *Cryogenics*, Vol. 31, No. 4, 1991, pp. 248–251.

[6]Ahlborn, K., "Durability of Carbon Fibre Reinforced Plastics with Thermoplastic Matrices Under Cyclic Mechanical and Cyclic Thermal Loads at Cryogenic Temperatures," *Cryogenics*, Vol. 31, No. 4, 1991, pp. 257–260.

[7]Ahlborn, K., "Cryogenic Mechanical Response of Carbon Fibre Reinforced Plastics with Thermoplastic Matrices to Quasi-Static Loads," *Cryogenics*, Vol. 31, No. 4, 1991, pp. 252–256.

[8]Schutz, J. B., "Properties of Composite Materials for Cryogenic Applications," *Cryogenics*, Vol. 38, No. 1, 1998, pp. 3–12.

[9]Schoeppner, G. A., Kim, R., and Donaldson, S. L., "Steady State Cracking of PMC's at Cryogenic Temperatures," AIAA Paper 2001-1216, April 2001.

[10]Shimoda, T., "Study of CFRP Application to the Cryogenic Propellant Tank of Reusable Launch Vehicle," AIAA Paper 2001-1598, April 2001.

[11]Kampf, G., *Characterization of Plastics by Physical Methods, Experimental Techniques, and Practical Application*, Hanser, Munich, 1986, Chap. 6.

[12]Suppliers of Advanced Composite Materials Association, *SACMA Recommended Methods*, Composites Fabricators Association, Arlington, VA, 1999.

[13]Council, N. R. (ed.), *U.S. Supersonic Commercial Aircraft*, National Academy Press, Washington, DC, 1997.

[14]"Strain Gage Selection," Vishay Intertechnology, Inc., TN 505, Malvern, PA, 1999.

[15]Jones, R. M., *Mechanics of Composite Materials*, Scripta, Washington, DC, 1975, Chap. 4.

[16]Johnson, T. F., and Gates, T. S., "High Temperature Polyimide Materials in Extreme Temperature Environments," AIAA Paper 2001-1214, April 2001.

[17]Herakovich, C. T., *Mechanics of Fibrous Composites*, Wiley, New York, 1998, p. 205.

K. Shivakumar
Associate Editor